analytical chemistry

pubs.acs.org/ac Article

First-Principles Collision Cross Section Measurements of Large Proteins and Protein Complexes

Jacob W. McCabe, Christopher S. Mallis, Klaudia I. Kocurek, Michael L. Poltash, Mehdi Shirzadeh, Michael J. Hebert, Liqi Fan, Thomas E. Walker, Xueyun Zheng, Ting Jiang, Shiyu Dong, Cheng-Wei Lin, Arthur Laganowsky, and David H. Russell*

Cite This: *Anal. Chem.* 2020, 92, 11155–11163 Read Online

ACCESS | Metrics & More | Article Recommendations | Supporting Information

ABSTRACT: Rotationally averaged collision cross section (CCS) values for a series of proteins and protein complexes ranging in size from 8.6 to 810 kDa are reported. The CCSs were obtained using a native electrospray ionization drift tube ion mobility-Orbitrap mass spectrometer specifically designed to enhance sensitivity while having high-resolution ion mobility and mass capabilities. Periodic focusing (PF)-drift tube (DT)-ion mobility (IM) provides first-principles determination of the CCS of large biomolecules that can then be used as CCS calibrants. The experimental, first-principles CCS values are compared to previously reported experimentally determined and computationally calculated CCS using projected superposition approximation (PSA), the Ion Mobility Projection Approximation Calculation Tool (IMPACT), and Collidoscope. Experimental CCS values are generally in agreement with previously reported CCSs, with values falling within ~5.5%. In addition, an ion mobility resolution (CCS centroid divided by CCS fwhm) of ~60 is obtained for pyruvate kinase (MW ~ 233 kDa); however, ion mobility resolution for bovine serum albumin (MW ~ 68 kDa) is less than ~20, which arises from sample impurities and underscores the importance of sample quality. The high resolution afforded by the ion mobility-Orbitrap mass analyzer provides new opportunities to understand the intricate details of protein complexes such as the impact of post-translational modifications (PTMs), stoichiometry, and conformational changes induced by ligand binding.

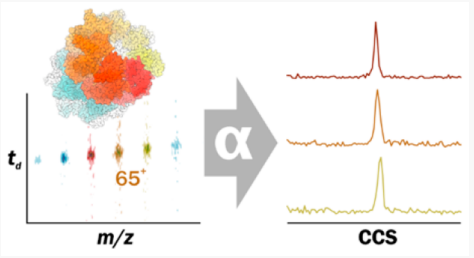

The arsenal of techniques currently used for studies of biomolecular structure, viz., circular dichroism (CD) spectroscopy,[1] nuclear magnetic resonance (NMR) spectroscopy,[2,3] X-ray crystallography (XRD),[4,5] and cryogenic-electron microscopy (CryoEM),[6,7] have undergone major advancements over the past few decades. These advances are complemented by parallel advances in mass spectrometry (MS)-based methods, including hydrogen/deuterium exchange (HDX),[8,9] hydroxyl radical footprinting (FPOP),[10,11] and increased numbers of covalent-labeling strategies.[12] Rapid progress has also been realized in the development of top-down protein sequencing strategies,[13,14] and similar approaches incorporating surface-induced dissociation (SID) make complex-down approaches for the determination of the stoichiometry and topology of protein complexes possible.[15−17] These latter MS-based approaches have occurred in parallel with the increased adoption of native MS, which aims to preserve the noncovalent interactions in the gas phase.[18,19]

Native MS,[18,19] a rapid and exquisitely sensitive technique, is now capable of providing information on protein complex subunit stoichiometry,[20−23] topology,[24−26] assembly pathways,[27,28] and individual ligand binding events.[29] Possibly of even greater significance for native MS is the ability to assess protein purity over traditional gel-based approaches.[30] Native ion mobility-mass spectrometry (IM-MS) makes studies of protein structure possible[31,32] as well as shows how interactions with metal ions,[33,34] small molecules,[35,36] protein tags,[37] proteins,[29] and nucleic acids[38] alter protein structure(s). An important feature of IM-MS is the ability to directly measure individual conformers that may comprise a population of gas-phase structures and the rotationally averaged collision cross sections (CCSs) that can be related to conformation and structural dynamics.[39−41] Software deconvolution of IM-MS data can allow for previously unresolved isomeric mixtures to be exposed using automated ion mobility deconvolution (AIMD).[42−44] When combined with collision-induced unfolding (CIU)[45] and variable-temperature electrospray ionization (vT-ESI),[46,47] it is possible to accurately determine gas- and solution-phase stabilities of the ions, respectively, along with conformational changes that occur upon ligand binding and/or changes of the local environment.[46−50]

Although IM-MS instrumentation developed during the proteomics era represent major technological advances, these

Received: March 24, 2020
Accepted: July 14, 2020
Published: July 14, 2020

https://dx.doi.org/10.1021/acs.analchem.0c01285
Anal. Chem. 2020, 92, 11155−11163

instruments impose significant limitations on the studies of large (i.e., >100 kDa), intact biological assemblies.[35,36,51,52] To circumvent these limitations, new IM-MS technologies with increased ion mobility and mass resolution are being developed; specifically, the Waters SELECT SERIES Cyclic IMS[53] and the native ESI-Fourier transform (FT) IM-Orbitrap MS possess the unique potential for high-resolution structural characterization of large biomolecules.[35−37,51,52,54−57]

Because the operation of the periodic focusing (PF)-drift tube (DT)-FT-IM Orbitrap instrument differs from typical commercial IM-MS instruments, a brief description of the instrument operation is included here. The instrument employs a dual-gate configuration to overcome the inherent duty-cycle mismatch for the PF-DT (tens of milliseconds) and the Orbitrap (hundreds of milliseconds).[51,55,58] Ion gates positioned at the entrance and exits of the DT are used to synchronously modulate the ion beam, which allows for operation of the DT as a frequency dispersive device. Ion drift frequencies of 5 Hz to 5 kHz correspond to ion drift times of 200 ms to 200 μs, respectively. In the FT-IMS mode, it is possible to acquire arrival time distributions (ATDs) and CCS for *every* ion present in a given mass spectrum in a single 8 min linear frequency sweep.

Here, the capabilities of a home-built PF-DT-FT-IM coupled to an Orbitrap mass spectrometer are critically evaluated with respect to the determination of CCS of soluble proteins and protein complexes ranging in size from 8.6 to 810 kDa. The reported CCS values are determined from first-principles using the modified Mason-Schamp equation,[59] and these values are compared with those previously reported and calculated from X-ray and CryoEM structures using the Ion Mobility Projection Approximation Calculation Tool (IMPACT),[60] projected superposition approximation (PSA),[61−64] and Collidoscope.[65]

EXPERIMENTAL SECTION

Chemicals and Materials. Soluble protein samples were purchased from Sigma-Aldrich or Fisher Scientific in lyophilized form and diluted to 1 mg/mL in 18.2 MΩ·cm water (Table S1). TTR and GroEL were expressed and purified as previously described.[66,67] The proteins were buffer exchanged using Micro Bio-Spin P-6 Gel Columns (Bio-Rad) into 200 mM ammonium acetate, and working concentrations were adjusted to 1 to 5 μM. Several microliters of protein solution were backloaded into pulled borosilicate tips prepared in-house from borosilicate capillaries (Sutter Instruments, BF150-86-10) using a micropipette puller (Sutter Instruments, P1000).

Instrumentation. Here, we describe modifications to the previously developed PF-DT-FT-IM[35,36,51] Orbitrap that increase our capabilities for native IM-MS, especially for studies of large protein complexes. Specifically, the 58 cm PF-DT has been extended to 1.5 m, thereby increasing the IM resolution. Increasing the DT length requires floating the ESI source an additional 1 kV higher, and to minimize the effects of Paschen breakdown, all source housing components were fabricated from Delrin acetal polymer. In addition, a second calibrated manometer was added to the end of the 1.5 m PF-DT to ensure carrier gas pressure (He, 99.999% purity) is constant throughout the length of the PF-DT.

Data Processing. Data files were processed as previously described.[35,36,51] In brief, custom in-house Python scripts utilized *multiplierz*[68] to extract from Thermo RAW files mass spectral data from each scan over the entire acquisition. Ion mobility data were obtained by extracting intensity information for m/z values over acquisition time followed by Fourier transform to convert from frequency to drift time domains using Scipy[69] and Numpy[70] packages. The resulting data can then be imported into UniDec[71] or PULSAR[72] for additional processing.

Ion Trajectory Simulations. SIMION (v8.1) ion trajectory simulations for ubiquitin (Ubq), transthyretin (TTR), and pyruvate kinase (PK) were performed under the low field limit, where the energy gained between collisions is less than the thermal energy of the collision gas for Ubq.[73] The simulations were limited to the specific design of the current PF-DT, where the lens thickness, spacing, and diameter are 6.35, 6.35, and 8.00 mm, respectively.[74−77] These dimensions give rise to fringing E-fields that radially confines ions as they traverse the PF-DT. The details and potential deleterious effects of collisional heating of the ions by the radial focusing have been described previously.[78,79]

Calculation of Collision Cross Section. First-principles CCSs (Ω) were calculated using the Mason-Schamp equation[59] (eq 1) along with the ion mobility dampening term, α, proposed previously[74] and described further in the main text.

$$\Omega = \alpha\left(\frac{3q}{16N_o}\right)\left(\frac{2\pi}{\mu k_b T}\right)^{1/2}\left(\frac{t_d E}{L}\right)\left(\frac{P_o T}{P T_o}\right) \quad (1)$$

where q is the charge of the ion, N_o is the standard particle density of the buffer gas, μ is the reduced mass of the ion and the buffer gas, k_b is Boltzmann's constant, T is the temperature in the drift tube, t_d is the drift time of the ion, E is the electric field strength, L is the length of the drift tube set herein as the distance between the two ion gates, P is the pressure inside the drift tube, and P_o and T_o are the standard pressure and temperature, respectively. Ions with equivalent CCSs will have longer drift times in PF-DT than those in UF-DT due to the distance-dependent oscillations and focusing throughout the IM separation. Therefore, without accounting for the mobility dampening term (α), the CCS for PF-DT would be systematically larger than that acquired using a UF-DT.

Ion ATDs obtained by the dual-gate setup used in eq 1 are an *exact* measure of the drift time of the ions between the two gates, thus eliminating the need for a multielectric field calibration (1/V plots)[80−82] to correct the measured ATD that ions spend outside of the drift tube. In addition, as long as the ions sampled by the second gate do not undergo dissociation or fragmentation, any postmobility changes in conformation will not impact the measured ATDs.

Uncertainties in CCS measurements obtained using the PF-DT were calculated on the basis of the standard deviation of 6 replicates for each protein or protein complex as recommended by Gabelica et al.[82] Day-to-day reproducibility of CCS was tested using transthyretin and was found to differ by less than 3% (data not shown). The temperature of the laboratory where these measurements were performed is maintained at ∼21 °C (70 ± 2 °F).

Collision Cross Section Determination from PDB Files. Atomic coordinates were downloaded from the PDB (www.rcsb.org) and visualized using PyMOL.[83−85] Biological assemblies were generated, if necessary, using crystallographic symmetry operators in PyMOL. Reference PDB codes for each protein and protein complex can be found in Table 1. PDB

https://dx.doi.org/10.1021/acs.analchem.0c01285
Anal. Chem. 2020, 92, 11155−11163

Table 1. Summary of CCS Values for Replicate Measurements (n = 6) as Compared to Other Methods Using the $\alpha_{E/N}$ Mobility Dampening Term Vide Supra[47,102,117−119] [a]

Protein Name	Mass (kDa)	z(+)	PF-DT CCS (nm^2)	u(CCS) (%)	K_o (cm^2/V·s)	K_o/z	CCS Lit (nm^2)	IMPACT (nm^2)	PSA (nm^2)	Collidoscope (nm^2)	PDB Code
Ubiquitin	8.558	4	10.8	3.04	1.73	4.32E-01	10.0	10.9	10.7	11.2	1UBQ
Lysozyme	14.30	6	14.2	1.94	1.97	3.28E-01	13.6	14.6	13.2	13.6	1AKI
Myoglobin	17.56	7	17.7	2.57	1.83	2.61E-01	17.2	17.1	16.3	17.9	1WLA
β-Lactoglobulin	18.35	7	17.8	1.90	1.83	2.62E-01	16.6	17.4	17.8	18.2	1BEB
2 β-Lactoglobulin	36.71	12	29.5	1.20	1.83	3.06E-01	29.0	31.2	27.9	31.8	2Q2M
Strep	51.88	13	34.9	1.03	1.78	1.37E-01	33.4	37.0	34.3	38.1	4Y5D
TTR	55.75	14	36.3	0.53	1.83	1.30E-01	34.1	36.9	34.6	37.8	1F41
Hemoglobin	64.48	16	40.3	1.04	1.91	1.19E-01	43.2	42.0	40.6	43.5	2QSS
BSA	68.81	14	45.7	1.88	1.49	1.06E-01	40.9	51.2	44.2	51.8	3V03
Concanvalin A	102.9	18	57.7	0.20	1.50	8.35E-02	0.0	61.1	56.3	62.9	3QLQ
ADH	148.2	23	73.6	0.52	1.51	6.29E-02	69.4	82.9	74.9	83.9	4W6Z
Aldolase	157.1	23	79.8	0.80	1.39	6.04E-02	76.1	88.6	79.1	89.1	6ALD
Pyruvate Kinase	233.4	31	109.7	1.70	1.38	4.46E-02	103.0	115.3	-	116.2	1F3W
GroEL	810.1	63	239.8	2.01	1.41	2.24E-02	209.0	305.3	-	292.7	1SS8

[a]Experimental CCS values are highlighted in red font for easier comparison. Masses listed are experimentally determined values. A more complete list of references for sources of experimental CCS values is noted in Table S1.

files were prepared for CCS calculations using PyMOL by removing water molecules and other cosolutes with explicit hydrogens added before exporting the structures for CCS determination. Heme cofactors were not removed from the structures.

Correction factors proposed by Hall et al. were originally implemented to correct for underestimation of projection approximation (PA) CCS values obtained from MOBCAL, by scaling the PA CCS output values to the ratio of experimental and PDB molecular weights.[86] Each of the CCS calculation tools utilized herein provides CCSs that are closely correlated to experimental CCSs and do not suggest scaling factors for missing atoms coordinated in the published methods.

For IMPACT[60] and Collidoscope,[65] atomic coordinates were exported from PyMOL as .PDB files. For PSA,[61−64] structures were exported as .xyz files. Default parameters were used for IMPACT, and the TJM* results of six trials were averaged. Default parameters were used for Collidoscope using 10 energy states and a temperature of 298 K. The input charge states for Collidoscope were the lowest observed charge states from the MS experiments. Default parameters were used for PSA with an input temperature of 298 K. PSA calculations were performed on the PSA WebServer (v0.5.1, psa.chem.fsu.edu).

RESULTS AND DISCUSSION

The Fourier transform IM-MS instrument used for this study incorporates several novel features, viz., a periodic-focusing IM drift tube (PF-DT) coupled to an extended mass range (EMR) Orbitrap mass spectrometer. The instrument and its operation as an FT-IM-MS platform have been described previously.[35,36,51] Originally developed by Gillig et al. in 2004, the PF-DT has increased ion transmission owing to radial focusing of the ions during the IM separation, and this has proved especially impactful for studies of large, multiply charged ions (>100 kDa).[87] That is, as the ions drift through the PF-DT, they experience a position-dependent E-field with an effective time-dependent field that is determined by the velocity and charge of the ion.[78,88,89] The radial focusing characteristics of the PF-DT are similar to both TWIMS[90] and RF-confining uniform field (RF-UF) DT.[87,89] Gamage et al. were able to explicitly derive an effective potential model for the PF-DT that describes changes in the electric fields as a function of distance, which were then used to determine deviations from the uniform field (UF) trajectories owing to the oscillatory (nonlinear) trajectories of ions in the PF drift field.[88] Silveira et al. derived an ion drift time damping term (α) that accounts for deviations in the drift times for ions in PF-DT as compared to UF-DT,[74,78,88] which can be directly applied to the Mason-Schamp equation to calculate first-principles CCS.[59]

The mobility damping term (α) applies to all classes of analytes, as shown previously with C_{60}^+, peptides, and denatured proteins;[74,89] Poltash et al. previously showed the utility of PF-DT for the analysis of protein complexes, i.e., TTR (MW 55.75 kDa).[35,36,51] CCSs were not reported in that study because the effects of α on the ATDs of native proteins or protein complexes ions had not been completed.[91] SIMION 8.1 simulations were performed to probe the relationship between α and reduced electric fields (E/N), denoted as $\alpha_{E/N}$, allowing for the calculation of the first-principles CCSs of native proteins and protein complexes. Trajectories for ubiquitin, transthyretin, and pyruvate kinase were simulated using *collision_hs1.lua*[92] (Figure S1) to probe native protein and protein complexes over a range of molecular weights, charge states, and pressures (1.00 to 2.30 Torr) to obtain the ATDs for both PF-DT and UF-DT.[74] The simulated CCS/ATDs can be used to determine α as shown in eq 2:[88]

$$\alpha \approx \frac{CCS_{PF-DT}}{CCS_{UF-DT}} \approx \frac{ATD_{UF-DT}}{ATD_{PF-DT}} \quad (2)$$

where CCS is the CCS obtained via eq 1 for both PF-DT and UF-DT and ATD is the arrival time distribution (s) of the ion packet in both the PF-DT and UF-DT.

Figure 1 contains plots of α versus reduced electric field (E/N) for simulated ion trajectories for proteins varying in molecular weight and charge. Generally, all three ions exhibit less radial motion (α approaches 1) with increasing E/N; however, as E/N decreases, the ions experience a linear decrease in α owing to the change in pressure. Deviations from linearity at lower E/N are attributed to ions spending more time between the electrodes, leading to increased numbers of collisions.[78,88,89] Error bars, shown in Figure 1, represent the propagated error ($\pm 1\sigma$) in the simulated ion arrival time distribution from both PF-DT and UF-DT.

https://dx.doi.org/10.1021/acs.analchem.0c01285
Anal. Chem. 2020, 92, 11155−11163

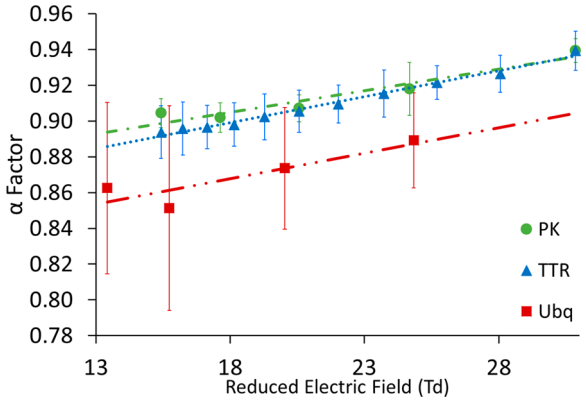

Figure 1. Calculated α values obtained for ubiquitin (red square, ~8 kDa), transthyretin (blue triangles, ~56 kDa tetramer), and pyruvate kinase (green circles, ~257 kDa tetramer) versus the reduced electric field (E/N). These plots illustrate the dependence of α on the pressure and electric field. Note that larger proteins exhibit less radial motion than low molecular weight proteins at higher He pressure, leading to increasing α values with increasing molecular weight. By correlating α as a function of pressure, α can now be estimated over a range of electric fields and pressures.

The magnitude of the error bars of $\alpha_{E/N}$ for ubiquitin increases as E/N decreases (Figure 1) and is directly correlated to the amplitude of the oscillatory motion ($X-Y$ plane, where Z is the direction of the applied E-field) of the ions in the PF-DT, which can lead to broadening of the ATD (see Figure S1). Simulations of both TTR and PK show a linear decrease that approaches an α value of approximately 0.89 and 0.91, respectively, at E/N of 15 Td. Proteins having similar size generally have similar charge state distributions, thus resulting in similar α values;[93] however, ion shapes, i.e., prolate, spherical, and oblate (vide infra), are also a contributor to ion ATDs.[94−98] Silveira et al. described the effect that charge has on the expected α, where higher charge ions have less radial motion and increased focusing of ions.[74] However, SIMION simulations show that, when the charge state of a protein approaches 15^+ (e.g., TTR and heavier), α approaches unity, and increasing the charge of the protein does not significantly impact α. For example, the effects of the distance-dependent pseudo-RF E-field on heavy, multiply charged ions, viz., pyruvate kinase (MW 233.4 kDa), are diminished, shown by the ion trajectories having less radial motion and increased ion focusing. This effect is similar to the stabilities of ion trajectories in an RF quadrupole where heavier complexes are more strongly influenced by the DC bias than by the applied RF potential, and the inverse is true for lower mass ions.[78,88] Ion trajectory simulations clearly demonstrate: (1) efficient radial focusing between each electrode, consistent with previous results for peptides and denatured proteins,[35,74,78,88,89] (2) increased ion transmission for PF compared to UF (data not shown), and (3) amplified radial

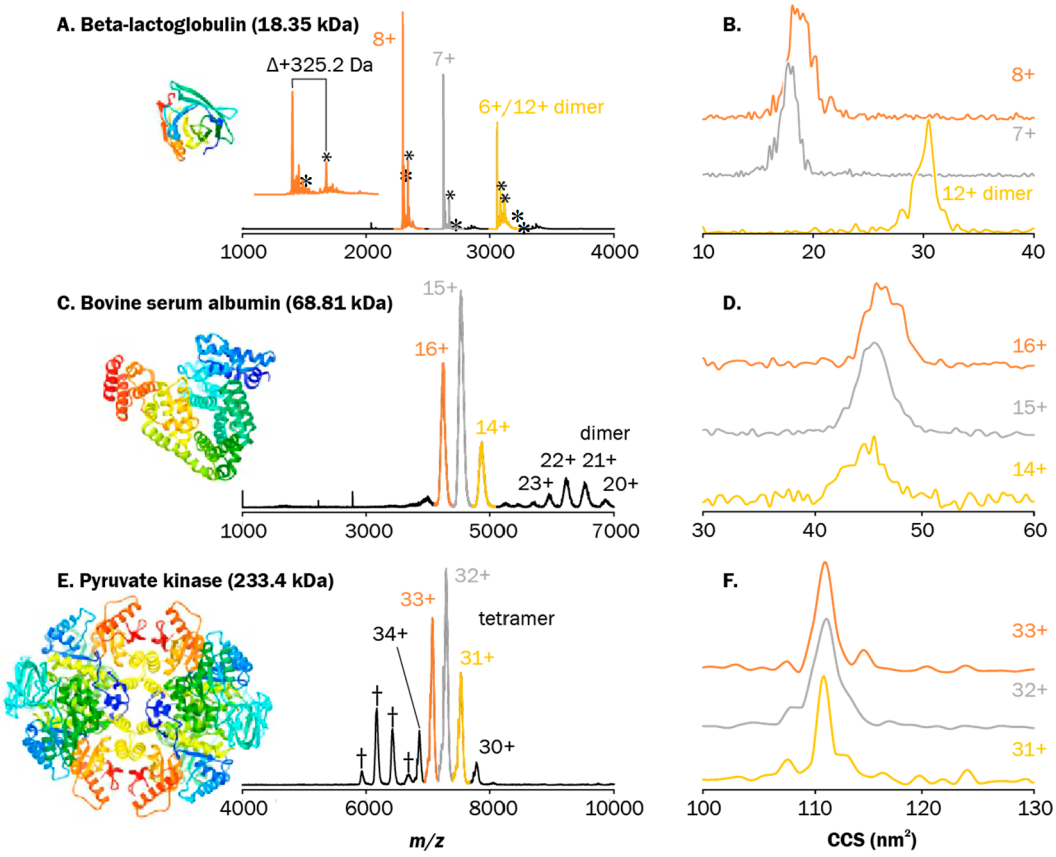

Figure 2. Native mass spectra and CCS profiles for β-lactoglobulin (PDB: 1BEB) (A, B), bovine serum albumin (PDB: 4F5S) (C, D), and pyruvate kinase (PDB: 1F3W) (E, F).[99−101] The peaks in the mass spectrum of BLG denoted by * correspond to a bound disaccharide (+325.2 Da). The widths of the peaks in the mass spectrum of BSA are broadened owing to some unknown impurities. Similarly, the peaks in the CCS profiles are also broadened owing to either sample impurities and/or conformational heterogeneity. Peaks denoted by † in the pyruvate kinase sample are impurities in the sample with an average mass of 154 kDa.

https://dx.doi.org/10.1021/acs.analchem.0c01285
Anal. Chem. 2020, 92, 11155−11163

focusing and increased transmission for large protein systems carrying large numbers of charges.

First-Principles Determination of CCS. Experimental ATDs were used to calculate CCS values using eq 1 and the $\alpha_{E/N}$ values derived from SIMION 8.1 (Figure 1). The $\alpha_{E/N}$ is applied as a function of MW of the protein, by categorizing proteins as small (<20 kDa), medium (<70 kDa), and large (>100 kDa) in a similar fashion to the $\alpha(z)$ previously reported by Silveira et al.[74]

Figure 2 contains structures, mass spectra, and CCS profiles for β-lactoglobulin A monomer (BLG, 18.35 kDa), bovine serum albumin (BSA, 68.81 kDa), and pyruvate kinase (PK, 233.4 kDa). BLG, BSA, and PK are used as examples of small (<20 kDa), medium (<70 kDa), and large (>100 kDa) molecular weight proteins, respectively, that have been used as model proteins in previous studies and are listed in various reference CCS databases.[102] The mass resolving power of the Orbitrap allows for baseline separation of intact BLG as well as BLG bound to an endogenous ligand[103] with a mass of 325.2 Da (Figure 2A). Notably, using low resolving power instruments previously employed, the ligated form of BLG may not be sufficiently resolved to obtain a clean CCS profile(s).[104] Note also that signals for BLG^{6+} and $2BLG^{12+}$ ions are isobaric, and orthogonal separations using IM are needed to confidently assign these signals. On the basis of the calculated CCS for the $2BLG^{12+}$ ions (Figure 2B), this signal is assigned to the dimer. The CCS for the BLG monomer is 17.8 nm^2 as compared to 29.5 nm^2 for $2BLG^{12+}$, and both are in excellent agreement (1.9%) with previously reported RF-UF values.[102]

The importance of mass resolving power is further illustrated by the analysis of BSA. Close inspection of MS signals of BSA suggests that they are significantly broadened compared to the expected isotope distribution (Figure 2C), possibly owing to unresolved protein-adduct ions. Note also that the CCS profiles for BSA 14^+ and 16^+ charge states are quite broad (Figure 2D). Possible sources for peak broadening are (i) unresolved adduct ions as observed for BLG in the m/z domain and/or (ii) heterogeneity of the structure of the ion that is further complicated by these observed adducts in the mass domain. To address this issue, several BSA samples were analyzed using a UHMR Orbitrap instrument.[105] The high-resolution mass spectra contained abundant signals for Cu-adducted BSA ions, whereas many as 10 Cu were observed (see Figures S2−S4).

The mass spectrum of PK (Figure 2E) contains abundant signals for the intact tetramer (with charge states of $30-34^+$). Low abundance, partially resolved signals from contaminates are also observed on the EMR platform. While the resolving power of the EMR Orbitrap is not sufficient to resolve these ions, they are fully resolved on the UHMR Orbitrap (see Figure S5). The deconvolution of the UHMR data shows contamination in the sample with a mass of ∼154 kDa. CCS values obtained for the three most abundant tetrameric ions (PK^{31+} to PK^{33+}) were 109.7 ± 1.7, 109.9 ± 0.1, and 110.0 ± 0.6 nm^2, respectively (Figure 2F). These CCS were obtained by extracting the ATDs for the regions of the m/z peak that do not overlap with the partially resolved signals.

Collectively, the data contained in Figure 2 demonstrate the capabilities of the FT-IMS-Orbitrap instrument for studies of small to large biomolecular ions. Figure 2 also demonstrates a similar sensitivity for a 1.5 m PF-DT when compared to the shorter, 58 cm PF-DT.[51] In addition to being able to analyze higher MW complexes, an ion mobility resolution (centroid divided by CCS fwhm) of ∼60 for PK was obtained due to this increased length of the DT, which to our knowledge is the highest DT-IM resolution reported for a large, intact native protein complex.

Benchmarking CCS to Other Methods. Figure 3 contains the comparison of $\alpha_{E/N}$ corrected CCS values

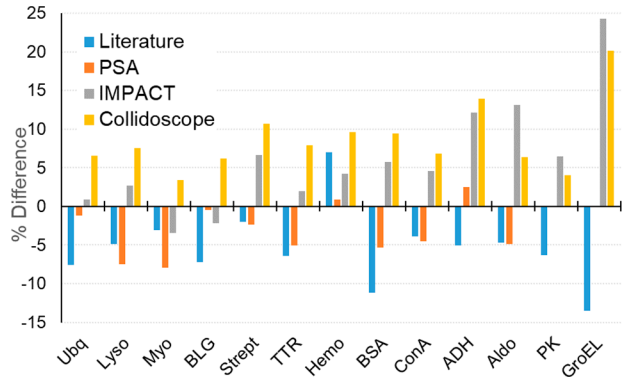

Figure 3. Percent differences of $\alpha_{E/N}$ corrected PF-DT CCS values vs literature experimental values and calculated CCS values from IMPACT, PSA, and Collidoscope for soluble proteins that span a range of molecular weights from 8.6 to 810 kDa. The CCSs were obtained using $\alpha_{E/N}$ corrected from Figure 2, using the lowest charge state of each protein in 200 mM ammonium acetate to be able to benchmark to previous literature values.[47,102,104,117,118]

obtained by using the PF-DT to previously published CCS first-principles and CCS values computationally calculated from atomic coordinates obtained from XRD using PSA, IMPACT, and Collidoscope.[99−102,106−116] The positive/negative percent differences correspond to a *larger/smaller* percent difference in the CCS of the respective methods from the PF-DT calculated CCS. As an example, the CCS of BSA calculated via IMPACT is 5.7% larger than the PF-DT CCS value. A complete listing of CCS values and PDB codes reported in Figure 3 are listed in Table 1, and CCS for all the detected charge states of these proteins can be found in Table S2. In general, the $\alpha_{E/N}$ corrected PF-DT CCS values are on average 5.5% larger than experimental CCS values obtained using RF-confining uniform field (RF-UF), with increased deviation as the MW of the proteins increases. On average, PF-DT and calculated CCS differed by +8.3%, −2.3%, and +8.0% than those calculated using IMPACT, PSA, and Collidoscope, respectively.

GroEL, a homotetradecameric protein complex (n = 14), was used to critically evaluate the performance of the IM-Orbitrap for the analysis of larger protein complexes. The charge states of GroEL vary, depending on the solution/buffer conditions, and it is unclear as to whether these changes altered the structure of the GroEL complex.[104,118] The MS data collected of GroEL via the PF-DT show a higher experimental mass than the theoretical mass (802.1 kDa, UniProt: P0A6F5)[120] that may be attributed to water, salts, or other adducts trapped inside the GroEL cavity. Zero-charge MS data was compiled for various instrument configurations and activating conditions in Table S3. Previously reported CCSs for GroEL were obtained from ammonium acetate solutions, and the CCSs (210 to 270 nm^2) are significantly smaller than the calculated CCS (∼300 nm^2).[102] Figure 4 contains native MS and IM-MS data for GroEL showing: (A)

https://dx.doi.org/10.1021/acs.analchem.0c01285
Anal. Chem. 2020, 92, 11155−11163

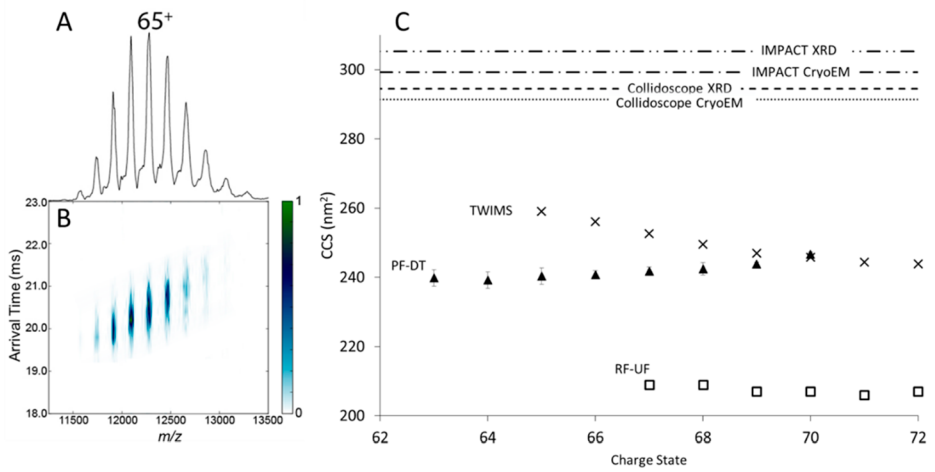

Figure 4. (A) Mass spectra, (B) ATD vs mass plots, and (C) CCS vs CSD (n = 6 replicate measurements) of native GroEL 14-mer complex with comparisons to PF-DT, TWIMS, RF-UF, Collidoscope, and IMPACT using both CryoEM (PDB: 5W0S) and XRD (PDB: 1SS8) structures.[106,107] CCSs of each charge state for 14 mer GroEL as compared to IMPACT and Collidoscope (for both XRD and CryoEM) as well as TWIMS (Heck and co-workers[104]) and RF-UF (Bush and co-workers[102]).

mass spectra (charge states centered at 65^+), (B) ATD vs m/z plot, and (C) a plot of experimental PF-DT CCS values (n = 6 replicate measurements) for the most abundant charge states versus previously reported experimental values (TWIMS and RF-UF). Also shown in this figure are the calculated CCS values (Collidoscope and IMPACT) for GroEL structures obtained from cryo-EM (PDB: 5W0S) and XRD (PDB: 1SS8) structures.[106,107]

The CCS obtained using PF-DT of 240 ± 5 nm^2 for the 63^+ charge state of GroEL is 24% and 20% smaller than that calculated by IMPACT using structures obtained by XRD and cryo-EM, respectively. These differences are also smaller (20% and 19%, respectively) than the Collidoscope calculated CCS. In both cases, the calculated values are considerably larger than the CCS obtained using PF-DT. There appears to be a small increase in the CCS obtained by using PF-DT as the charge state increases; however, the CCS obtained by TWIMS decreases as the charge state increases.[104] It is generally observed that the CCS increases with increasing charge, but to our knowledge, neither trend for CCS vs charge state has been broadly applicable for protein complexes.

The smaller experimental CCS suggests that the gas-phase ions have significantly different shapes from GroEL molecules that are trapped in virtuous ice or a rigid crystal lattice. Previous studies have shown that the apical domain of GroEL is highly flexible, and this flexibility is what allows ATP-dependent binding of the GroES to GroEL (group 1 chaperonins), resulting in the transition from a "barrel" to a prolated "football" like structure.[97,98,121−123] A similar flexibility of the apical domain is found for Group 2 chaperonins that do not require GroES for function or formation of prolate "football" shapes.[114] Thus, we attribute the differences between the experimental and calculated CCSs to differences in shapes of these ions. Ewing et al. explained these differences by invoking the formation of collapsed conformers during the transition from solution to the gas phase;[65] however, we estimate that a "closed" (prolate) conformation formed by changes in the orientation of the apical domain would have a smaller CCS than would an "open" conformation.[97,98] In fact, the GroEL ions sampled here are not fully dehydrated. For example, the mass of the GroEL ions we observed differs from the theoretical molecular weight by ∼8000 Da, viz., 810.1 vs 802.1 kDa, a mass difference that Heck and co-workers attributed to "...trapping water molecules, buffer molecules and salt within the protein complex".[104] Preliminary results suggest that the water, buffer molecules, and salts present do not have a structural role. For example, mild collisional heating of the GroEL 65^+ ions can be used to remove these adducted species from the 810.1 kDa GroEL ions, and the resulting 802.1 kDa GroEL ions also have a CCS of ∼240 nm^2. Thus, the disparity between the experimental and calculated CCSs for gas-phase ions and structures of condensed phase structures (cryo-EM and XRD)[117,118] warrant more extensive experimental and computational investigations.

CONCLUSION

The PF-DT-FT-IMS-Orbitrap instrument takes advantage of radial focusing by the PF-DT, which increases the transmission of high charge state ions, and multiplexed data acquisition to overcome the duty-cycle mismatch of DT-IM and Orbitrap MS. Multiplexed acquisition also yields increased sensitivity owing to the inherent gains afforded by the Fellgett's or multiplexed advantage, viz., "more signal more of the time."[124] While traditional commercial IM time-of-flight (IM-ToF) instruments have made rapid developments in omics-related research possible, these instruments, unfortunately, fall short of the needs for the growing field of structural biology, viz., first-principles determinations of CCSs combined with high-resolution MS measurements of native, intact proteins and protein complexes.

First-principles determinations of CCSs of varying MW proteins and protein complexes (8.6−810 kDa) have been determined on a high-resolution PF-DT FT-IM-Orbitrap MS. The CCS values corrected for the mobility damping term, α, fall within 6% of previously published RF-UF values and within 2−8% of CCS values calculated from crystal structures using different methods. Transmission for large biomolecules is increased by using the PF-DT, in agreement with trajectory simulations obtained by using SIMON 8.1, thereby increasing the sensitivity of the PF-DT FT-IM-Orbitrap instrument. With smaller systems, sample complexity is not the limiting factor

https://dx.doi.org/10.1021/acs.analchem.0c01285
Anal. Chem. 2020, 92, 11155−11163

and the mass resolution of IM-ToF instruments is more than adequate for the identification of charge states, low MW adducts, and/or truncations, which has been extensively demonstrated.[35,36,51,52] The increased resolution offered on the PF-DT FT-IM-Orbitrap MS over traditional IM-ToF provides a modern means to ascertain the purity of proteins (vis-à-vis fewer post-translational modifications (PTMs), noncovalent adducts, truncations, metalation, etc.) that can impact the conformational dynamics of the proteins. With the technological advancements achieved with the PF-DT FT-IM-Orbitrap platform, the rigor for pure samples for IM standards to be used as calibrants is brought to the fore.

■ ASSOCIATED CONTENT

Supporting Information

The Supporting Information is available free of charge at https://pubs.acs.org/doi/10.1021/acs.analchem.0c01285.

Description of the SIMION calculation, high-resolution MS data for BSA and PK, and additional tables for CCS values for different charge states, protein source, and GroEL mass comparisons (PDF)

■ AUTHOR INFORMATION

Corresponding Author

David H. Russell − *Department of Chemistry, Texas A&M University, College Station, Texas 77843, United States;* orcid.org/0000-0003-0830-3914; Email: russell@chem.tamu.edu

Authors

Jacob W. McCabe − *Department of Chemistry, Texas A&M University, College Station, Texas 77843, United States;* orcid.org/0000-0002-5022-2280

Christopher S. Mallis − *Department of Chemistry, Texas A&M University, College Station, Texas 77843, United States*

Klaudia I. Kocurek − *Department of Chemistry, Texas A&M University, College Station, Texas 77843, United States*

Michael L. Poltash − *Department of Chemistry, Texas A&M University, College Station, Texas 77843, United States*

Mehdi Shirzadeh − *Department of Chemistry, Texas A&M University, College Station, Texas 77843, United States*

Michael J. Hebert − *Department of Chemistry, Texas A&M University, College Station, Texas 77843, United States*

Liqi Fan − *Department of Chemistry, Texas A&M University, College Station, Texas 77843, United States*

Thomas E. Walker − *Department of Chemistry, Texas A&M University, College Station, Texas 77843, United States*

Xueyun Zheng − *Department of Chemistry, Texas A&M University, College Station, Texas 77843, United States;* orcid.org/0000-0001-9782-4521

Ting Jiang − *Department of Chemistry, Texas A&M University, College Station, Texas 77843, United States;* orcid.org/0000-0002-8661-9714

Shiyu Dong − *Department of Chemistry, Texas A&M University, College Station, Texas 77843, United States*

Cheng-Wei Lin − *Department of Chemistry, Texas A&M University, College Station, Texas 77843, United States;* orcid.org/0000-0002-6917-8953

Arthur Laganowsky − *Department of Chemistry, Texas A&M University, College Station, Texas 77843, United States;* orcid.org/0000-0001-5012-5547

Complete contact information is available at: https://pubs.acs.org/10.1021/acs.analchem.0c01285

Notes

The authors declare no competing financial interest.

■ ACKNOWLEDGMENTS

The authors wish to thank Will Seward and Karl Yeager of the Texas A&M University Chemistry Machine Shop for the fabrication of the parts, Greg Matthijetz of the Texas A&M University Laboratory for Biological Mass Spectrometry for assisting in the configuration of the electronics, Dr. Andrew Roth and Dr. Hays Rye for providing the GroEL sample, and Dr. Alexander Makarov for the assistance in configuring IM to the Orbitrap. Funding for this work was provided by the National Science Foundation CHE-1707675 (D.H.R.), National Institutes of Health DP2GM123486 (A.L.), R01GM121751 (D.H.R. and A.L.), and P41GM1285771 (D.H.R.), and endowment funds from an MDS SCIEX Professorship (D.H.R.).

■ REFERENCES

(1) Wallace, B. A. *Curr. Opin. Struct. Biol.* **2019**, *58*, 191−196.
(2) Markwick, P. R. L.; Malliavin, T.; Nilges, M. *PLoS Comput. Biol.* **2008**, *4* (9), No. e1000168.
(3) van der Wel, P. C. A. *Emerg Top Life Sci.* **2018**, *2* (1), 57−67.
(4) Shi, Y. *Cell* **2014**, *159* (5), 995−1014.
(5) Zheng, H.; Handing, K. B.; Zimmerman, M. D.; Shabalin, I. G.; Almo, S. C.; Minor, W. *Expert Opin. Drug Discovery* **2015**, *10* (9), 975−989.
(6) Murata, K.; Wolf, M. *Biochim. Biophys. Acta, Gen. Subj.* **2018**, *1862* (2), 324−334.
(7) Bai, X.-c.; McMullan, G.; Scheres, S. H. W. *Trends Biochem. Sci.* **2015**, *40* (1), 49−57.
(8) Masson, G. R.; Burke, J. E.; Ahn, N. G.; Anand, G. S.; Borchers, C.; Brier, S.; Bou-Assaf, G. M.; Engen, J. R.; Englander, S. W.; Faber, J.; Garlish, R.; Griffin, P. R.; Gross, M. L.; Guttman, M.; Hamuro, Y.; Heck, A. J. R.; Houde, D.; Iacob, R. E.; Jørgensen, T. J. D.; Kaltashov, I. A.; Klinman, J. P.; Konermann, L.; Man, P.; Mayne, L.; Pascal, B. D.; Reichmann, D.; Skehel, M.; Snijder, J.; Strutzenberg, T. S.; Underbakke, E. S.; Wagner, C.; Wales, T. E.; Walters, B. T.; Weis, D. D.; Wilson, D. J.; Wintrode, P. L.; Zhang, Z.; Zheng, J.; Schriemer, D. C.; Rand, K. D. *Nat. Methods* **2019**, *16* (7), 595−602.
(9) Konermann, L.; Pan, J.; Liu, Y.-H. *Chem. Soc. Rev.* **2011**, *40* (3), 1224−1234.
(10) Kiselar, J.; Chance, M. R. *Annu. Rev. Biophys.* **2018**, *47* (1), 315−333.
(11) Gau, B. C.; Sharp, J. S.; Rempel, D. L.; Gross, M. L. *Anal. Chem.* **2009**, *81* (16), 6563−6571.
(12) Mendoza, V. L.; Vachet, R. W. *Mass Spectrom. Rev.* **2009**, *28* (5), 785−815.
(13) Donnelly, D. P.; Rawlins, C. M.; DeHart, C. J.; Fornelli, L.; Schachner, L. F.; Lin, Z.; Lippens, J. L.; Aluri, K. C.; Sarin, R.; Chen, B.; Lantz, C.; Jung, W.; Johnson, K. R.; Koller, A.; Wolff, J. J.; Campuzano, I. D. G.; Auclair, J. R.; Ivanov, A. R.; Whitelegge, J. P.; Paša-Tolić, L.; Chamot-Rooke, J.; Danis, P. O.; Smith, L. M.; Tsybin, Y. O.; Loo, J. A.; Ge, Y.; Kelleher, N. L.; Agar, J. N. *Nat. Methods* **2019**, *16* (7), 587−594.
(14) Catherman, A. D.; Skinner, O. S.; Kelleher, N. L. *Biochem. Biophys. Res. Commun.* **2014**, *445* (4), 683−693.
(15) Stiving, A. Q.; VanAernum, Z. L.; Busch, F.; Harvey, S. R.; Sarni, S. H.; Wysocki, V. H. *Anal. Chem.* **2019**, *91* (1), 190−209.
(16) Zhou, M.; Wysocki, V. H. *Acc. Chem. Res.* **2014**, *47* (4), 1010−1018.
(17) VanAernum, Z. L.; Gilbert, J. D.; Belov, M. E.; Makarov, A. A.; Horning, S. R.; Wysocki, V. H. *Anal. Chem.* **2019**, *91* (5), 3611−3618.
(18) Chandler, S. A.; Benesch, J. L. P. *Curr. Opin. Chem. Biol.* **2018**, *42*, 130−137.

(19) Leney, A. C.; Heck, A. J. R. *J. Am. Soc. Mass Spectrom.* **2017**, *28* (1), 5−13.
(20) Benesch, J. L. P.; Aquilina, J. A.; Ruotolo, B. T.; Sobott, F.; Robinson, C. V. *Chem. Biol.* **2006**, *13* (6), 597−605.
(21) Hernández, H.; Robinson, C. V. *Nat. Protoc.* **2007**, *2* (3), 715−726.
(22) Rajabi, K.; Ashcroft, A. E.; Radford, S. E. *Methods* **2015**, *89*, 13−21.
(23) Zilkenat, S.; Grin, I.; Wagner, S. *Biol. Chem.* **2017**, *398*, 155.
(24) Patterson, A.; Tokmina-Lukaszewska, M.; Bothner, B. Chapter Five - Probing Cascade complex composition and stability using native mass spectrometry techniques. In *Methods in Enzymology*; Bailey, S., Ed.; Academic Press: 2019; Vol. *616*, pp 87−116.
(25) Sahasrabuddhe, A.; Hsia, Y.; Busch, F.; Sheffler, W.; King, N. P.; Baker, D.; Wysocki, V. H. *Proc. Natl. Acad. Sci. U. S. A.* **2018**, *115*, 1268.
(26) Taverner, T.; Hernández, H.; Sharon, M.; Ruotolo, B. T.; Matak-Vinković, D.; Devos, D.; Russell, R. B.; Robinson, C. V. *Acc. Chem. Res.* **2008**, *41* (5), 617−627.
(27) Levy, E. D.; Erba, E. B.; Robinson, C. V.; Teichmann, S. A. *Nature* **2008**, *453* (7199), 1262−1265.
(28) Bleiholder, C.; Bowers, M. T. *Annu. Rev. Anal. Chem.* **2017**, *10* (1), 365−386.
(29) Hyung, S.-J.; Robinson, C. V.; Ruotolo, B. T. *Chem. Biol.* **2009**, *16* (4), 382−390.
(30) Laemmli, U. K. *Nature* **1970**, *227* (5259), 680−685.
(31) Majuta, S. N.; Maleki, H.; Kiani Karanji, A.; Attanyake, K.; Loch, E.; Valentine, S. J. *Curr. Opin. Chem. Biol.* **2018**, *42*, 101−110.
(32) Ben-Nissan, G.; Sharon, M. *Curr. Opin. Chem. Biol.* **2018**, *42*, 25−33.
(33) Chen, S.-H.; Chen, L.; Russell, D. H. *J. Am. Chem. Soc.* **2014**, *136* (26), 9499−9508.
(34) Chen, S.-H.; Russell, D. H. *Biochemistry* **2015**, *54* (39), 6021−6028.
(35) Poltash, M. L.; McCabe, J. W.; Shirzadeh, M.; Laganowsky, A.; Russell, D. H. *TrAC, Trends Anal. Chem.* **2020**, *124*, 115533.
(36) Poltash, M. L.; Shirzadeh, M.; McCabe, J. W.; Moghadamchargari, Z.; Laganowsky, A.; Russell, D. H. *Chem. Commun.* **2019**, *55* (28), 4091−4094.
(37) Shirzadeh, M.; Poltash, M. L.; Laganowsky, A.; Russell, D. H. *Biochemistry* **2020**, *59*, 1013.
(38) Poltash, M. L.; Shirzadeh, M.; McCabe, J. W.; Moghadamchargari, Z.; Laganowsky, A.; Russell, D. H. *Chem. Commun. (Cambridge, U. K.)* **2019**, *55* (28), 4091−4094.
(39) Wyttenbach, T.; von Helden, G.; Batka, J. J.; Carlat, D.; Bowers, M. T. *J. Am. Soc. Mass Spectrom.* **1997**, *8* (3), 275−282.
(40) May, J. C.; Morris, C. B.; McLean, J. A. *Anal. Chem.* **2017**, *89* (2), 1032−1044.
(41) Paglia, G.; Angel, P.; Williams, J. P.; Richardson, K.; Olivos, H. J.; Thompson, J. W.; Menikarachchi, L.; Lai, S.; Walsh, C.; Moseley, A.; Plumb, R. S.; Grant, D. F.; Palsson, B. O.; Langridge, J.; Geromanos, S.; Astarita, G. *Anal. Chem.* **2015**, *87* (2), 1137−1144.
(42) Harper, B.; Neumann, E. K.; Stow, S. M.; May, J. C.; McLean, J. A.; Solouki, T. *Anal. Chim. Acta* **2016**, *939*, 64−72.
(43) Pettit, M. E.; Harper, B.; Brantley, M. R.; Solouki, T. *Analyst* **2015**, *140* (20), 6886−6896.
(44) Brantley, M.; Zekavat, B.; Harper, B.; Mason, R.; Solouki, T. *J. Am. Soc. Mass Spectrom.* **2014**, *25* (10), 1810−1819.
(45) Dixit, S. M.; Polasky, D. A.; Ruotolo, B. T. *Curr. Opin. Chem. Biol.* **2018**, *42*, 93−100.
(46) El-Baba, T. J.; Clemmer, D. E. *Int. J. Mass Spectrom.* **2019**, *443*, 93−100.
(47) Woodall, D. W.; Brown, C. J.; Raab, S. A.; El-Baba, T. J.; Laganowsky, A.; Russell, D. H.; Clemmer, D. E. *Anal. Chem.* **2020**, *92* (4), 3440−3446.
(48) Cong, X.; Liu, Y.; Liu, W.; Liang, X.; Russell, D. H.; Laganowsky, A. *J. Am. Chem. Soc.* **2016**, *138* (13), 4346−9.
(49) Marchand, A.; Rosu, F.; Zenobi, R.; Gabelica, V. *J. Am. Chem. Soc.* **2018**, *140*, 12553−12565.
(50) Clemmer, D. E.; Russell, D. H.; Williams, E. R. *Acc. Chem. Res.* **2017**, *50* (3), 556−560.
(51) Poltash, M. L.; McCabe, J. W.; Shirzadeh, M.; Laganowsky, A.; Clowers, B. H.; Russell, D. H. *Anal. Chem.* **2018**, *90* (17), 10472−10478.
(52) Poltash, M. L.; McCabe, J. W.; Patrick, J. W.; Laganowsky, A.; Russell, D. H. *J. Am. Soc. Mass Spectrom.* **2019**, *30* (1), 192−198.
(53) Giles, K.; Ujma, J.; Wildgoose, J.; Pringle, S.; Richardson, K.; Langridge, D.; Green, M. *Anal. Chem.* **2019**, *91* (13), 8564−8573.
(54) Knorr, F. J.; Eatherton, R. L.; Siems, W. F.; Hill, H. H. *Anal. Chem.* **1985**, *57* (2), 402−406.
(55) Morrison, K. A.; Siems, W. F.; Clowers, B. H. *Anal. Chem.* **2016**, *88* (6), 3121−3129.
(56) Clowers, B. H.; Ibrahim, Y.; Prior, D. C.; Danielson, W. F.; Belov, M.; Smith, R. D. *Anal. Chem.* **2008**, *80* (3), 612−623.
(57) Liu, Y.; LoCaste, C. E.; Liu, W.; Poltash, M. L.; Russell, D. H.; Laganowsky, A. *Nat. Commun.* **2019**, *10* (1), 1352.
(58) Clowers, B. H.; Hill, H. H. *Anal. Chem.* **2005**, *77* (18), 5877−5885.
(59) Mason, E. A.; McDaniel, E. W. *NASA STI/Recon Technical Report A* **1988**, *89*, 15174.
(60) Marklund, E. G.; Degiacomi, M. T.; Robinson, C. V.; Baldwin, A. J.; Benesch, J. L.P. *Structure* **2015**, *23* (4), 791−799.
(61) Bleiholder, C.; Wyttenbach, T.; Bowers, M. T. *Int. J. Mass Spectrom.* **2011**, *308* (1), 1−10.
(62) Bleiholder, C.; Contreras, S.; Do, T. D.; Bowers, M. T. *Int. J. Mass Spectrom.* **2013**, *345*−*347*, 89−96.
(63) Anderson, S. E.; Bleiholder, C.; Brocker, E. R.; Stang, P. J.; Bowers, M. T. *Int. J. Mass Spectrom.* **2012**, *330*−*332*, 78−84.
(64) Bleiholder, C.; Contreras, S.; Bowers, M. T. *Int. J. Mass Spectrom.* **2013**, *354*−*355*, 275−280.
(65) Ewing, S. A.; Donor, M. T.; Wilson, J. W.; Prell, J. S. *J. Am. Soc. Mass Spectrom.* **2017**, *28* (4), 587−596.
(66) Shirzadeh, M.; Boone, C. D.; Laganowsky, A.; Russell, D. H. *Anal. Chem.* **2019**, *91* (3), 2345−2351.
(67) Weaver, J.; Jiang, M.; Roth, A.; Puchalla, J.; Zhang, J.; Rye, H. S. *Nat. Commun.* **2017**, *8* (1), 15934.
(68) Alexander, W. M.; Ficarro, S. B.; Adelmant, G.; Marto, J. A. *Proteomics* **2017**, *17* (15−16), 1700091.
(69) Virtanen, P.; Gommers, R.; Oliphant, T. E.; Haberland, M.; Reddy, T.; Cournapeau, D.; Burovski, E.; Peterson, P.; Weckesser, W.; Bright, J.; van der Walt, S. J.; Brett, M.; Wilson, J.; Millman, K. J.; Mayorov, N.; Nelson, A. R. J.; Jones, E.; Kern, R.; Larson, E.; Carey, C. J.; Polat, İ.; Feng, Y.; Moore, E. W.; VanderPlas, J.; Laxalde, D.; Perktold, J.; Cimrman, R.; Henriksen, I.; Quintero, E. A.; Harris, C. R.; Archibald, A. M.; Ribeiro, A. H.; Pedregosa, F.; van Mulbregt, P.; Vijaykumar, A.; Bardelli, A. P.; Rothberg, A.; Hilboll, A.; Kloeckner, A.; Scopatz, A.; Lee, A.; Rokem, A.; Woods, C. N.; Fulton, C.; Masson, C.; Häggström, C.; Fitzgerald, C.; Nicholson, D. A.; Hagen, D. R.; Pasechnik, D. V.; Olivetti, E.; Martin, E.; Wieser, E.; Silva, F.; Lenders, F.; Wilhelm, F.; Young, G.; Price, G. A.; Ingold, G.-L.; Allen, G. E.; Lee, G. R.; Audren, H.; Probst, I.; Dietrich, J. P.; Silterra, J.; Webber, J. T.; Slavič, J.; Nothman, J.; Buchner, J.; Kulick, J.; Schönberger, J. L.; de Miranda Cardoso, J. V.; Reimer, J.; Harrington, J.; Rodríguez, J. L. C.; Nunez-Iglesias, J.; Kuczynski, J.; Tritz, K.; Thoma, M.; Newville, M.; Kümmerer, M.; Bolingbroke, M.; Tartre, M.; Pak, M.; Smith, N. J.; Nowaczyk, N.; Shebanov, N.; Pavlyk, O.; Brodtkorb, P. A.; Lee, P.; McGibbon, R. T.; Feldbauer, R.; Lewis, S.; Tygier, S.; Sievert, S.; Vigna, S.; Peterson, S.; More, S.; Pudlik, T.; Oshima, T.; Pingel, T. J.; Robitaille, T. P.; Spura, T.; Jones, T. R.; Cera, T.; Leslie, T.; Zito, T.; Krauss, T.; Upadhyay, U.; Halchenko, Y. O.; Vázquez-Baeza, Y.; SciPy, C. *Nat. Methods* **2020**, *17* (3), 261−272.
(70) van der Walt, S.; Colbert, S C.; Varoquaux, G. *Comput. Sci. Eng.* **2011**, *13* (2), 22−30.
(71) Marty, M. T.; Baldwin, A. J.; Marklund, E. G.; Hochberg, G. K. A.; Benesch, J. L. P.; Robinson, C. V. *Anal. Chem.* **2015**, *87* (8), 4370−4376.

https://dx.doi.org/10.1021/acs.analchem.0c01285
Anal. Chem. 2020, 92, 11155−11163

(72) Allison, T. M.; Reading, E.; Liko, I.; Baldwin, A. J.; Laganowsky, A.; Robinson, C. V. *Nat. Commun.* **2015**, *6* (1), 8551.
(73) Verbeck, G. F.; Ruotolo, B. T.; Gillig, K. J.; Russell, D. H. *J. Am. Soc. Mass Spectrom.* **2004**, *15* (9), 1320−1324.
(74) Silveira, J. A.; Jeon, J.; Gamage, C. M.; Pai, P.-J.; Fort, K. L.; Russell, D. H. *Anal. Chem.* **2012**, *84* (6), 2818−2824.
(75) Silveira, J. A.; Gamage, C. M.; Blase, R. C.; Russell, D. H. *Int. J. Mass Spectrom.* **2010**, *296* (1−3), 36−42.
(76) Gamage, C. M.; Silveira, J. A.; Blase, R. C.; Russell, D. H. *Int. J. Mass Spectrom.* **2011**, *303* (2−3), 154−163.
(77) Blase, R. C.; Silveira, J. A.; Gillig, K. J.; Gamage, C. M.; Russell, D. H. *Int. J. Mass Spectrom.* **2011**, *301* (1−3), 166−173.
(78) Silveira, J. A.; Gamage, C. M.; Blase, R. C.; Russell, D. H. *Int. J. Mass Spectrom.* **2010**, *296* (1−3), 36−42.
(79) Fort, K. L.; Silveira, J. A.; Russell, D. H. *Anal. Chem.* **2013**, *85* (20), 9543−9548.
(80) Stow, S. M.; Causon, T. J.; Zheng, X.; Kurulugama, R. T.; Mairinger, T.; May, J. C.; Rennie, E. E.; Baker, E. S.; Smith, R. D.; McLean, J. A.; Hann, S.; Fjeldsted, J. C. *Anal. Chem.* **2017**, *89* (17), 9048−9055.
(81) Cole, R. B. *Electrospray and MALDI mass spectrometry: fundamentals, instrumentation, practicalities, and biological applications*; John Wiley & Sons: 2011.
(82) Gabelica, V.; Shvartsburg, A. A.; Afonso, C.; Barran, P.; Benesch, J. L. P.; Bleiholder, C.; Bowers, M. T.; Bilbao, A.; Bush, M. F.; Campbell, J. L.; Campuzano, I. D. G.; Causon, T.; Clowers, B. H.; Creaser, C. S.; De Pauw, E.; Far, J.; Fernandez-Lima, F.; Fjeldsted, J. C.; Giles, K.; Groessl, M.; Hogan, C. J.; Hann, S.; Kim, H. I.; Kurulugama, R. T.; May, J. C.; McLean, J. A.; Pagel, K.; Richardson, K.; Ridgeway, M. E.; Rosu, F.; Sobott, F.; Thalassinos, K.; Valentine, S. J.; Wyttenbach, T. *Mass Spectrom. Rev.* **2019**, *38* (3), 291−320.
(83) Schrodinger, LLC *The AxPyMOL Molecular Graphics Plugin for Microsoft Power Point*, Version 1.8; 2015.
(84) Schrodinger, LLC *The JyMOL Molecular Graphics Development Component*, Version 1.8; 2015.
(85) Schrodinger, LLC *The PyMOL Molecular Graphics System*, Version 1.8; 2015.
(86) Hall, Z.; Politis, A.; Robinson, C. V. *Structure* **2012**, *20* (9), 1596−1609.
(87) Gillig, K. J.; Ruotolo, B. T.; Stone, E. G.; Russell, D. H. *Int. J. Mass Spectrom.* **2004**, *239* (1), 43−49.
(88) Gamage, C. M.; Silveira, J. A.; Blase, R. C.; Russell, D. H. *Int. J. Mass Spectrom.* **2011**, *303* (2−3), 154−163.
(89) Blase, R. C.; Silveira, J. A.; Gillig, K. J.; Gamage, C. M.; Russell, D. H. *Int. J. Mass Spectrom.* **2011**, *301* (1−3), 166−173.
(90) Dixit, S. M.; Richardson, K.; Langridge, D.; Giles, K.; Ruotolo, B. T. *J. Am. Soc. Mass Spectrom.* **2020**, *31*, 880.
(91) Poltash, M. L.; McCabe, J. W.; Shirzadeh, M.; Laganowsky, A.; Clowers, B. H.; Russell, D. H. *Anal. Chem.* **2018**, *90* (17), 10472−10478.
(92) Manura, D.; Dahl, D. *SIMION (R) 8.0 User Manual*; Scientific Instrument Services, Inc.: Ringoes, NJ 08551, 2008; http://simion.com.
(93) Kaltashov, I. A.; Mohimen, A. *Anal. Chem.* **2005**, *77* (16), 5370−5379.
(94) Ruotolo, B. T.; Gillig, K. J.; Woods, A. S.; Egan, T. F.; Ugarov, M. V.; Schultz, J. A.; Russell, D. H. *Anal. Chem.* **2004**, *76* (22), 6727−6733.
(95) McLean, J. A.; Ruotolo, B. T.; Gillig, K. J.; Russell, D. H. *Int. J. Mass Spectrom.* **2005**, *240* (3), 301−315.
(96) McLean, J. A. *J. Am. Soc. Mass Spectrom.* **2009**, *20* (10), 1775−1781.
(97) Hewitt, D.; Marklund, E.; Scott, D. J.; Robinson, C. V.; Borysik, A. J. *J. Phys. Chem. B* **2014**, *118* (29), 8489−8495.
(98) Landreh, M.; Sahin, C.; Gault, J.; Sadeghi, S.; Drum, C. L.; Uzdavinys, P.; Drew, D.; Allison, T. M; Degiacomi, M. T.; Marklund, E. G. *Anal. Chem.* **2020**, DOI: 10.1021/acs.analchem.0c01940.
(99) Brownlow, S.; Cabral, J. H. M.; Cooper, R.; Flower, D. R.; Yewdall, S. J.; Polikarpov, I.; North, A. C. T.; Sawyer, L. *Structure* **1997**, *5* (4), 481−495.
(100) Majorek, K. A.; Porebski, P. J.; Dayal, A.; Zimmerman, M. D.; Jablonska, K.; Stewart, A. J.; Chruszcz, M.; Minor, W. *Mol. Immunol.* **2012**, *52* (3), 174−182.
(101) Wooll, J. O.; Friesen, R. H. E.; White, M. A.; Watowich, S. J.; Fox, R. O.; Lee, J. C.; Czerwinski, E. W. *J. Mol. Biol.* **2001**, *312* (3), 525−540.
(102) Bush, M. F.; Hall, Z.; Giles, K.; Hoyes, J.; Robinson, C. V.; Ruotolo, B. T. *Anal. Chem.* **2010**, *82* (22), 9557−9565.
(103) Fenaille, F.; Morgan, F.; Parisod, V.; Tabet, J.-C.; Guy, P. A. *J. Mass Spectrom.* **2004**, *39* (1), 16−28.
(104) Duijn, E. v.; Barendregt, A.; Synowsky, S.; Versluis, C.; Heck, A. J. R. *J. Am. Chem. Soc.* **2009**, *131* (4), 1452−1459.
(105) Fort, K. L.; van de Waterbeemd, M.; Boll, D.; Reinhardt-Szyba, M.; Belov, M. E.; Sasaki, E.; Zschoche, R.; Hilvert, D.; Makarov, A. A.; Heck, A. J. R. *Analyst* **2018**, *143* (1), 100−105.
(106) Chaudhry, C.; Horwich, A. L.; Brunger, A. T.; Adams, P. D. *J. Mol. Biol.* **2004**, *342* (1), 229−245.
(107) Roh, S.-H.; Hryc, C. F.; Jeong, H.-H.; Fei, X.; Jakana, J.; Lorimer, G. H.; Chiu, W. *Proc. Natl. Acad. Sci. U. S. A.* **2017**, *114* (31), 8259−8264.
(108) Terai, T.; Kohno, M.; Boncompain, G.; Sugiyama, S.; Saito, N.; Fujikake, R.; Ueno, T.; Komatsu, T.; Hanaoka, K.; Okabe, T.; Urano, Y.; Perez, F.; Nagano, T. *J. Am. Chem. Soc.* **2015**, *137* (33), 10464−10467.
(109) Choi, K. H.; Mazurkie, A. S.; Morris, A. J.; Utheza, D.; Tolan, D. R.; Allen, K. N. *Biochemistry* **1999**, *38* (39), 12655−12664.
(110) Raj, S. B.; Ramaswamy, S.; Plapp, B. V. *Biochemistry* **2014**, *53* (36), 5791−5803.
(111) Trastoy, B.; Bonsor, D. A.; Pérez-Ojeda, M. E.; Jimeno, M. L.; Méndez-Ardoy, A.; García Fernández, J. M.; Sundberg, E. J.; Chiara, J. L. *Adv. Funct. Mater.* **2012**, *22* (15), 3191−3201.
(112) Aranda IV, R.; Cai, H.; Worley, C. E.; Levin, E. J.; Li, R.; Olson, J. S.; Phillips Jr, G. N.; Richards, M. P. *Proteins: Struct., Funct., Genet.* **2009**, *75* (1), 217−230.
(113) Hörnberg, A.; Eneqvist, T.; Olofsson, A.; Lundgren, E.; Sauer-Eriksson, A. E. *J. Mol. Biol.* **2000**, *302* (3), 649−669.
(114) Maurus, R.; Overall, C. M.; Bogumil, R.; Luo, Y.; Mauk, A. G.; Smith, M.; Brayer, G. D. *Biochim. Biophys. Acta, Protein Struct. Mol. Enzymol.* **1997**, *1341* (1), 1−13.
(115) Al-Karadaghi, S.; Hansson, M.; Nikonov, S.; Jönsson, B.; Hederstedt, L. *Structure* **1997**, *5* (11), 1501−1510.
(116) Vijay-Kumar, S.; Bugg, C. E.; Cook, W. J. *J. Mol. Biol.* **1987**, *194* (3), 531−544.
(117) May, J. C.; Jurneczko, E.; Stow, S. M.; Kratochvil, I.; Kalkhof, S.; McLean, J. A. *Int. J. Mass Spectrom.* **2018**, *427*, 79−90.
(118) Stiving, A. Q.; Jones, B. J.; Ujma, J.; Giles, K.; Wysocki, V. H. *Anal. Chem.* **2020**, *92*, 4475.
(119) Valentine, S. J.; Counterman, A. E.; Clemmer, D. E. *J. Am. Soc. Mass Spectrom.* **1997**, *8* (9), 954−961.
(120) The UniProt Consortium. *Nucleic Acids Res.* **2019**, *47* (D1), D506−D515.
(121) Pereira, J. H.; Ralston, C. Y.; Douglas, N. R.; Meyer, D.; Knee, K. M.; Goulet, D. R.; King, J. A.; Frydman, J.; Adams, P. D. *J. Biol. Chem.* **2010**, *285* (36), 27958−27966.
(122) Koike-Takeshita, A.; Arakawa, T.; Taguchi, H.; Shimamura, T. *J. Mol. Biol.* **2014**, *426* (21), 3634−3641.
(123) Fei, X.; Ye, X.; LaRonde, N. A.; Lorimer, G. H. *Proc. Natl. Acad. Sci. U. S. A.* **2014**, *111* (35), 12775−12780.
(124) Fellgett, P. B. *J. Opt. Soc. Am.* **1949**, *39* (11), 970−976.